Available online at www.sciencedirect.com
SCIENCE DIRECT®
International Journal of Heat and Mass Transfer 47 (2004) 4365–4375
International Journal of HEAT and MASS TRANSFER
www.elsevier.com/locate/ijhmt

Experimental study of local thermal non-equilibrium phenomena during phase change in porous media

A.G. Agwu Nnanna [a,*], A. Haji-Sheikh [b], Kendall T. Harris [b]

[a] Department of Engineering, Purdue University, Calumet, Hammond, IN 46323-2094, USA
[b] Department of Mechanical and Aerospace Engineering, The University of Texas at Arlington, Arlington, TX 76019-0023, USA

Received 23 July 2003; received in revised form 15 April 2004

Abstract

This study presents a systematic experimental method of estimating the extent of the phase front under the local thermal non-equilibrium condition in porous media saturated with phase change materials (PCM). It describes a comparison of measured temperature of the solid matrix at pre-selected sites with the average pore temperature in order to substantiate the existence of the local thermal non-equilibrium condition. Also, the measured data are compared with the theoretical predictions reported in the literature. The agreement between the experimental and theoretical prediction is highly satisfactory. The results clearly show that, early during the phase change process, the Sparrow number is relatively small and the solid matrix is not at the local thermal equilibrium with the pore materials. At larger time, the Sparrow number rapidly increases and the system approaches the local thermal equilibrium condition.

1. Introduction

Thawing and freezing in porous media are often encountered in the field of science and engineering. These applications range from cryopreservation and cryosurgery of biological tissues, freezing of soil, and food preservation to thermal storage systems for passive cooling of electronic devices. Solidification in a flow through a porous medium is also commonly encountered in the formation of metal matrix composites by infiltration of molten metals into fibrous preforms of composite [1]. The moving boundary problems in homogeneous materials have been the subject of investigation for many decades [2]. A review of the literature indicates that very little work has been done to study the phase change phenomena in porous media under the condition of local thermal non-equilibrium (LTNE). Ellinger and Beckermann [3] reported an experimental study of the melting of a pure substance in a vertical rectangular enclosure that is partially occupied by horizontal or vertical layers of a relatively high thermal conductivity porous medium. They observed that the differences in thermophysical properties between the porous layer and the pure fluid layer have a strong effect on the movement and shape of the solid/liquid interface. Beckermann and Ellinger [4] investigated natural convection (solid/liquid phase change) in porous media by treating the entire domain as a single region governed by one set of conservation equations. They concluded that some deficiencies exist between results obtained from their mathematical and experimental models. Song and Viskanta [5] conducted a theoretical and experimental investigation of the lateral freezing of an anisotropic porous medium saturated with an aqueous salt solution. In their theoretical study, they assumed local thermal equilibrium (LTE) between the solid matrix and the fluid. They concluded that the porous matrix phase affected the freezing of an aqueous salt solution by offering an additional resistance to the motion of the fluid and migration of separated crystals. In a numerical and

* Corresponding author. Tel.: +1-219-989-2071; fax: +1-219-989-2898.

0017-9310/$ - see front matter © 2004 Published by Elsevier Ltd.
doi:10.1016/j.ijheatmasstransfer.2004.04.029

Nomenclature

A	surface area, m^2
C	$C = \varepsilon\overline{C}_p + (1-\varepsilon)C_s$, $J\,m^{-3}\,K^{-1}$
CB	containment box
$\overline{C}_p$	mean heat capacitance of materials in pores, $J\,m^{-3}\,K^{-1}$
C_s	solid heat capacitance, $J\,m^{-3}\,K^{-1}$
h	interstitial heat transfer coefficient, $W\,m^{-2}\,K^{-1}$
H	porous layer thickness, m
k	thermal conductivity, W/m K
L	latent heat of fusion, J/kg
LTE	local thermal equilibrium
LTNE	local thermal non-equilibrium
PCM	phase change material
r	τ_t/τ_a
R_c	contact resistance, $m^2\,K\,W^{-1}$
r	position vector, m
S	volumetric heat source, $W\,m^{-3}$
SD	standard deviation
SMTP	solid matrix temperature probe
Sp	Sparrow number, $hX^2/(k_e r_h)$
t	time, s
T_m	phase change temperature, K
T_0	surface temperature at $x = 0$, K
T_p	mean temperature of pore materials, K
T_s	solid matrix temperature, K
x, y, z	coordinates, m
X	location of the front, m
X^*	$X\sqrt{2\rho L/[\pi\tau_a k_e(T_0 - T_m)]}$
V	volume, m^3

Greek symbols

α	thermal diffusivity, k_e/C, $m^2\,s^{-1}$
ε	V_f/V
η	τ_t/τ_a
θ_p	$(T_p - T_m)/(T_0 - T_m)$
θ_s	$(T_s - T_m)/(T_0 - T_m)$
ξ	$x/\sqrt{\alpha\tau_a}$
ρ	density, $kg\,m^{-3}$
τ_a	$C_s\tau_t/C + \tau_q$
τ_e	$C_s\tau_t/C$
τ_q	lag time in heat flux, s
τ_t	lag time in temperature, s

Subscripts

c	contact
e	equivalent
h	hydraulic
l	liquid
p	pore
s	solid

experimental study on the freezing of a porous medium in contact with a concentrated aqueous freezant, Lucas et al. [6] analyzed the heat and mass transport through the porous medium based on local thermal equilibrium. They attributed the discrepancy between their numerical and experimental results to their assumption of local thermodynamic phase equilibrium between the solid matrix and the fluid.

Previous investigations conducted on flow through porous media hypothesized that the solid matrix and the primary material within the pore satisfy the local thermal equilibrium condition, thus heat transfer parameters were predicted based on the isothermal condition. Sahraoui and Kaviany [7–9] reported a one-equation model of the heat transfer process associated with the boundary between the fluid and solid phase in the porous media. The existence of a local thermal equilibrium condition in porous media becomes uncertain for applications that involve rapid heating processes, and in nuclear reactor modeling where the temperature gradient between the fluid and solid matrix is significant. Ochoa-Tapia and Whitaker [10] reported heat transfer analysis based on a two-equation model at the boundary between a porous medium and a homogeneous fluid. They found that flux jump conditions exist between a porous medium and a homogeneous fluid when the condition of local thermal equilibrium is invalid and, as a result, separate transport equations are required for each phase. Recently, Vafai and Sozen [11] reported a two-phase equation model of flow through a porous medium. Results obtained from their study revealed a significant discrepancy between the fluid and solid phase temperature distribution.

The location of the phase front in porous media saturated with phase change material is often predicted based on the assumption of a local thermal equilibrium (LTE) condition. During the phase change process, it is expected that the temperature of the solid matrix encapsulating the pore will be higher than the temperature of the pore materials during melting and lower during freezing. Therefore, the assumption of a thermodynamic equilibrium condition during the phase change process is somewhat unrealistic. Therefore, this study emphasizes the investigation of thermodynamic non-equilibrium phenomena during phase change in porous media. In a theoretical investigation of the LTNE model [12] during phase change phenomena in porous media, an enthalpy model was developed to predict the extent of the phase change front during the phase change process. In that study, a two-equation

model, from Minkowycz et al. [13], was selected and applied to the differential element of a PCM-saturated porous medium to get

$$\varepsilon\frac{\partial H_p(\mathbf{r},t)}{\partial t} = -\nabla\cdot\mathbf{q}_p(\mathbf{r},t) + ha_c(T_s - T_p) + S_p(\mathbf{r},t) \quad (1)$$

$$(1-\varepsilon)C_s\frac{\partial T_s(\mathbf{r},t)}{\partial t} = -\nabla\cdot\mathbf{q}_s(\mathbf{r},t) - ha_c(T_s - T_p) + S_s(\mathbf{r},t) \quad (2)$$

The subscripts "p" and "s" refer to the materials in the pores and the solid matrix, respectively, and $\mathbf{r}$ is the position vector. The parameter $H_p(\mathbf{r},t)$ is local enthalpy per unit volume, h is the interstitial heat transfer coefficient, ε is the porosity, $a_c = \varepsilon/r_h$, and $r_h = V_p/A_p$ is the hydraulic radius. The function $S_p(\mathbf{r},t)$ and $S_s(\mathbf{r},t)$ are the contribution of a source or a sink within the primary phase and the solid matrix; in the absence of volumetric heat generation in the solid matrix, $S_p(\mathbf{r},t) = S_s(\mathbf{r},t) = 0$. The respective heat flux components by conduction are $\mathbf{q}_p(\mathbf{r},t)$ and $\mathbf{q}_s(\mathbf{r},t)$. After adding Eq. (1) to Eq. (2) and setting $\mathbf{q}(\mathbf{r},t) = \mathbf{q_p}(\mathbf{r},t) + \mathbf{q_s}(\mathbf{r},t)$, the result is

$$-\nabla\cdot\mathbf{q}(\mathbf{r},t) = \varepsilon\overline{C}_p\frac{\partial T_p(\mathbf{r},t)}{\partial t} + (1-\varepsilon)C_s\frac{\partial T_s(\mathbf{r},t)}{\partial t} \quad (3)$$

where $\mathbf{q}(\mathbf{r},t)$ is the applied heat flux. According to Tzou [14], prior to the onset of local thermal equilibrium, the Fourier thermal conduction model should be modified and replaced by the equation

$$\mathbf{q}(\mathbf{r},t) + \tau_q\frac{\partial\mathbf{q}(\mathbf{r},t)}{\partial t} = -k_e\left\{\nabla T_p(\mathbf{r},t) + \tau_t\frac{\partial}{\partial t}[\nabla T_p(\mathbf{r},t)]\right\} \quad (4)$$

where τ_q is the lag time in heat flux due to the solid-to-solid contact resistance and τ_t is the lag time in temperature due to the interstitial heat transfer coefficient h. Eliminating the heat flux vector $\mathbf{q}$ between Eqs. (3) and (4) results in the relation [13].

$$\nabla\cdot(k_e\nabla T_p) + \tau_t\frac{\partial[\nabla\cdot(k_e\nabla T_p)]}{\partial t} = C\left[\frac{\partial T_p}{\partial t} + (\tau_e+\tau_q)\frac{\partial^2 T_p}{\partial t^2}\right] \quad (5a)$$

since T_s and T_p are related [13] through the relation

$$T_s(x,t) = T_p(x,t) + \tau_t\frac{\partial T_p(x,t)}{\partial t} \quad (5b)$$

while $\tau_e = C_s\tau_t/C$, $\tau_a = \tau_e + \tau_q$, and $C = \varepsilon\overline{C}_p + (1-\varepsilon)C_s$.

In one-dimensional space, Ref. [12] defines a melt front X whose location is related to heat flux at $x = 0$; that is, $q(0,t) = -k_e\partial T_p/\partial x \cong \rho L\partial X/\partial t$ where L is the latent heat (J/kg). Based on Eqs. (3)–(5) and after some algebraic manipulations, the dimensionless phase front is expressed as

$$X^* = X\sqrt{2\rho L/[\pi\tau_a k_e(T_0 - T_m)]} \quad (6)$$

and it is related to t/τ_a and τ_t/τ_a where τ_a is related to τ_t, τ_q, and other thermophysical properties, see Ref. [12]. Minkowycz et al. [13] reported the Sparrow number Sp that would indicate the occurrence of LTNE condition. By selecting X as the characteristic length, the Sparrow number $Sp = hX^2/(k_e r_h)$ reduces to $Sp \cong \overline{C}_p X^2/(\tau_t k_e)$ since $\tau_t \approx r_h\overline{C}_p/h$ as given in [13].

The abovementioned methodology, as given in Ref. [12], is an effective method of predicting the location of a front during a LTNE phase change process. However, no experimental verification of this theoretical method is cited in the literature. This experimental study attempts to investigate the range of validity of the theoretical model in [12] to predict the location of the phase front. The primary focus of this paper is to provide sufficient experimental evidence of local thermal non-equilibrium phenomena during phase change in porous media and to experimentally investigate the theoretical model of the phase front X^*. The system selected for this investigation is a stagnant PCM-saturated porous medium. The temperature of the solid matrix is monitored at pre-selected sites during the phase change process. The measured temperature data are used to determine the phase front as a function of time and the results are compared with a modified theoretical prediction similar to that in Ref. [12].

2. Test facility and apparatus

2.1. Test setup

The test facility is depicted schematically in Fig. 1. It consists of five major parts: (1) test apparatus, (2) the water and heat supply system, (3) thermal chamber, (4) solid matrix temperature probe (SMTP), and (5) data acquisition system. The physical dimensions of the test apparatus are 127-mm long×127-mm wide×40-mm heigh, see Fig. 2. A 3.5-mm wide×40-mm long×1-mm thick perforated plate is mounted at the midpoint of the base of the test apparatus to hold the temperature probes in place during the experiment. The perforated plate has six vertically aligned 3.2-mm diameter holes

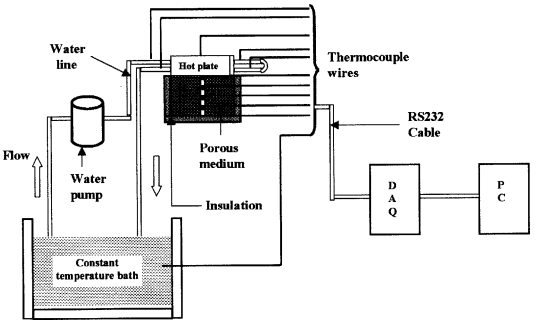

Fig. 1. Experimental facility.

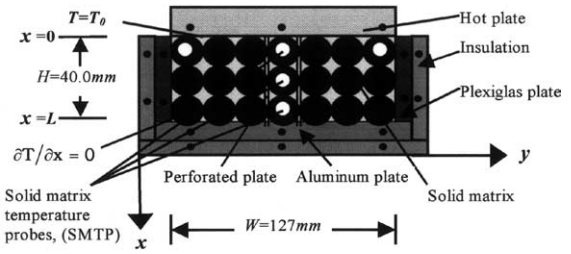

Fig. 2. Test apparatus for the transient experiment. The black dots are the locations of the thermocouple.

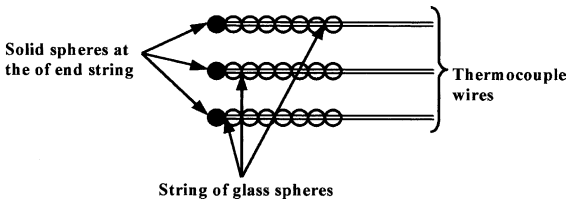

Fig. 3. Schematic of the SMTP.

at locations: $x = 4.46 \pm 0.25$, 9.8 ± 0.22, 16.39 ± 0.06, 22.18 ± 0.25, 28.33 ± 0.37, and 35.37 ± 0.11 mm. The test apparatus, including the perforated plate, are fabricated from acrylic Plexiglas material, a low thermal conductivity thermoplastic. Due to its low thermal conductivity value of 1.1 W/m K, the effect of lateral heat transfer from the sides of the test apparatus is negligible. All the external surfaces of the test apparatus, with the exception of the surface where the heat load is applied, were insulated with a 21.3-mm thick Styrofoam board in order to reduce heat losses from the sides to the surroundings. The thermal conductivity of Styrofoam over the range of temperature considered in this experiment is ~0.0224 W/m K.

The heat flux is applied at the top surface of the enclosure to minimize the effect of natural convection within porous media. The temperature of the hot plate is maintained at a near constant temperature by re-circulating hot water. The hot water is supplied by a constant temperature bath. As shown in Fig. 1, the variation in the bath temperature is ±0.5 °C. The constant temperature bath is connected to the isothermal hot plate via a piping network system. Hot water from the constant temperature bath is re-circulated to and from the hot plate using a hydraulic pump.

Prior to running an experiment, it is necessary to pre-heat the phase change materials to a pre-assigned constant temperature. The thermal chamber for pre-heating the porous medium is a Thermolyne Type-30400 automatic furnace. The furnace is heated by four electric resistance heaters, which are embedded in a refractory material. The chamber is insulated with ceramic fiber insulation. The temperature of the furnace is regulated using built-in controllers.

The temperature of the solid matrix is measured at pre-selected locations using a solid matrix temperature probe, SMTP, fabricated in-house within the Heat Transfer Laboratory at UTA. The selected thermocouples are copper-constant, 40-gage T-type. The thermocouple's head was placed inside of the solid glass sphere, shown as dark circles in Fig. 3. To avoid thermocouple wire interference during the melting/freezing process, the wire was passed through a string of hollow spheres, also shown in Fig. 3 but as white circles. Each string consists of a series of 3-mm outside diameter hollow spheres bonded to each other using thermally conductive paste. One end of the string is sealed and attached to a solid glass sphere using a thermal paste, OMEGABOND 101. The other end of the string is used for implantation of the thermocouple. Each SMTP is inserted into the holes on the perforated plate and is held in place with thermal grease. All the SMTPs were placed parallel to the isothermal plate to reduce heat loss by conduction through the thermocouple wire.

A total of 20 copper–constantan (Type T) thermocouples including the SMTPs were deployed to monitor temperature variations at pre-selected sites in the experimental facility. Within the porous medium, seven SMTPs were mounted on the perforated plate to monitor changes in temperature of the solid matrix, at the locations along the x-axis in the direction of heat flow. Two additional SMTPs were placed along other directions to verify one-dimensionality of the heat flow. Four thermocouples were attached to the isothermal plate, one on each side of the plate; one at each fluid inlet and exit to measure the respective temperatures. In addition, seven thermocouples are used to measure the temperature of the surroundings: one inserted into the water bath, two placed into the thermal chamber, two deployed to monitor the ambient temperature, and two attached to the insulation board to measure temperature across the insulation. The error in the thermocouple readings is estimated to be ±0.2 °C and verified under constant temperature condition while the test model is in the constant temperature chamber.

All the thermocouple wires, including the SMTPs, were connected to a 20-channel Reed plug-in module with built-in temperature compensation for direct temperature measurement. The plug-in module communicates with the floating logic via the internal isolated digital bus of the data logger HP34970A. Temperature measurements from the data logger are automatically recorded in the personal computer for further data reduction.

2.2. Test procedure

As part of the preparation for the experimental run, the test apparatus is randomly packed with 3-mm

diameter solid glass spheres to form a non-consolidated porous medium with a porosity of 0.446. The thermal conductivity of the glass sphere is 1.3 W/m K. The test apparatus containing the porous medium is saturated with approximately 200 g of liquid phase tetracosane. Tetracosane (99% pure) is a PCM used in this study. It has a melting temperature of 49.5 °C, the thermal conductivity of the liquid phase is 0.17 W/m K, the thermal conductivity of the solid phase is 0.24 W/m K [15,16], the density at the melting temperature is 796 kg/m^3 [17], and the latent heat is 255 kJ/kg [17]. Using a guarded hot plate technique and steady state condition, the equivalent thermal conductivity of the PCM-saturated porous medium is measured at 0.55 W/m K, details are in Nnanna [18]. It compares well with the empirical relation in Kaviany [19]. The test apparatus is then filled with PCM and placed into a temperature-controlled thermal chamber (Thermolyne furnace Type-30400) for about 6 h to solidify. During the solidification process, adjustment was made so that the solidification begins at the lower surface and proceeds toward the upper surface. This procedure prevents the upper region from solidifying at a faster rate than the lower region, hence eliminating the formation of voids. Additional liquid tetracosane is periodically added to ensure that the porous medium is fully saturated, hence eliminating the presence of air in the pore. When the solidification process is complete, a preliminary temperature measurement is made to ascertain uniformity in temperature throughout the porous medium. This is accomplished by measuring the temperature of the SMTP embedded at the pre-selected locations.

As a prelude to a phase change experiment, the PCM-saturated medium along with the insulation were pre-heated in the thermal chamber to 47 °C, which is 2.5 °C below the melting temperature of the pore material. During the pre-heating process, which lasted for about 30 h, the temperature of the porous medium is constantly monitored using the SMTPs instrumented at pre-selected sites. The pre-heating process is complete once uniform temperature is established at all locations in the porous medium. Next, the isothermal hot plate is pre-heated by re-circulating hot water from the constant temperature bath to the hot plate via its internal piping network. Thermocouples attached to the isothermal plate monitor the changes in temperature until the desired temperature is reached, which is usually much higher than the melting temperature of the PCM.

The experimental simulation begins following the activation of the data acquisition system and placement of the pre-heated isothermal hot plate on the exposed surface of the pre-heated PCM-saturated porous medium. All the experiments were performed under standard laboratory conditions (room temperature and pressure). The duration for the simulation is 3500 s, and the sampling rate is 0.681 s for the 20 thermocouples location. A total of four sets of experiments were performed at pre-selected isothermal hot plate temperature $T_0 = 64.2$, 71.6, 80.3, and 89 °C. A set of experiments consists of three experiments performed at the same temperature T_0 to ensure reproducibility of the temperature data. All the temperature data were automatically transferred and recorded in a personal computer for further data analysis.

The main source of uncertainties in this study includes error due to the measurement of temperature and physical dimensions. The combined uncertainty of the data logger HP34970A and the thermocouple calibration in the measurement of temperature is ±0.4% or ±0.2 °C. The uncertainty in the caliper (Mitutoyo) for the measurement of the physical dimension of the test apparatus is ±0.02 mm.

3. Results and discussion

Figs. 4 and 5 illustrate a sample of temperature profiles of the solid matrix caused by the imposed isothermal surface conditions, at $x = 0$, for two data sets ($T_0 = 80.3$, 89 °C). In these figures, the thermal response of the solid matrix at the selected locations, and the temperature profile for the constant temperature hot plate are plotted. It can be seen that the response of the solid matrix in the near-field region was rapid while a finite time was required for the solid matrix in the far-field region to register a significant change in temperature. The thermal response time of the solid matrix increased with increasing distance away from the hot plate. This is not unprecedented since most of the energy deposited on the porous medium at $x = 0$ is consumed in the pore within the vicinity of the isothermal boundary as the latent heat of fusion. Because the heat of fusion for the pore material is much larger than the sensible heat of the solid matrix, the rate of change of

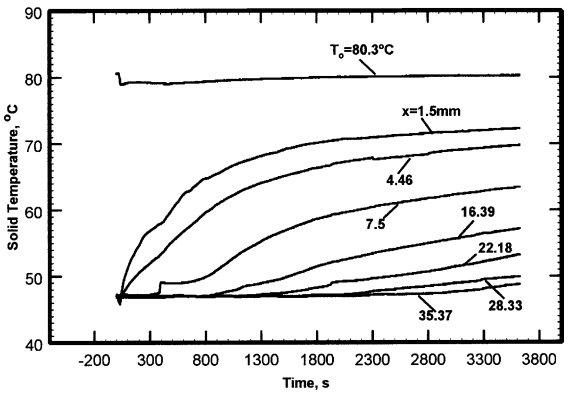

Fig. 4. Variation of temperature with time, PCM-saturated porous medium, $T_0 = 80.3$ °C.

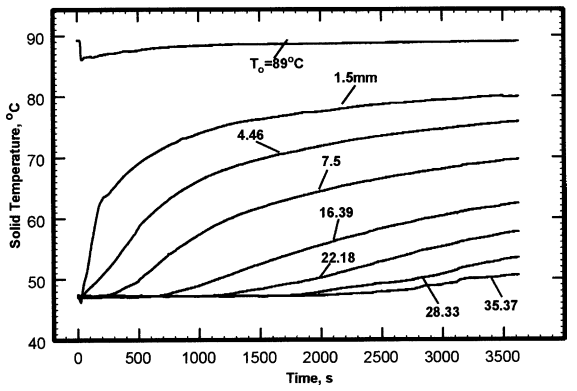

Fig. 5. Variation of temperature with time, PCM-saturated porous medium, $T_0 = 89$ °C.

temperature in the far-field region is small. Furthermore, since the porous medium was initially near the phase change temperature and the melting process is slow, any further heat addition to the medium will initiate the phase change process in the near-field region rather than increase the temperature in the far-field region.

An examination of data from Figs. 4 and 5 does not reveal the thermal equilibrium or non-equilibrium condition of the porous medium. One method of validating the condition of the porous medium is to compare the measured temperature of the solid with the average temperature of the pore material. Direct and accurate measurement of the transient response of the pore material to thermal disturbance is experimentally challenging if not impossible because of the relatively large temperature variation during melting and freezing. In one-dimensional space, using Eq. (5), an approximate theoretical enthalpy model, developed by Harris et al. [12] to study the phase change process in porous media, provides a method of calculating the average pore temperature T_p for LTNE condition using the energy equation,

$$\alpha\frac{\partial^2 T_p}{\partial x^2}+\alpha\tau_t\frac{\partial^3 T_p}{\partial t\partial x^2}=\frac{\partial T_p}{\partial t}+\tau_a\frac{\partial^2 T_p}{\partial t^2}\quad \text{for } 0\leqslant x<\infty \tag{7a}$$

where τ_t and τ_a relaxation times in Eq. (5). When $\tau_a = 0$ and $\tau_t = 0$, Eq. (7a) reduces to the classical Fourier heat conduction equation (LTE model). Therefore, τ_t and τ_a are finite in the presence of local thermal non-equilibrium condition.

Harris et al. [12] hypothesized that the effective capacitance during the phase change is independent of τ_t and τ_q. Therefore, when $r = \tau_t/\tau_a = 1$, Eq. (7a) reduces to

$$\left(1+\tau_t\frac{\partial}{\partial t}\right)\left(\alpha\frac{\partial^2 T_p}{\partial x^2}-\frac{\partial T_p}{\partial t}\right)=0\quad \text{for } 0\leqslant x<\infty \tag{7b}$$

The solution of Eq. (7b), subject to the conditions $T = T_m$ at $t = 0$ and $T = T_0$ at $x = 0$ when $t > 0$ is

$$T_p = T_m + (T_0 - T_m)\mathrm{erfc}\left(\frac{x}{\sqrt{4\alpha t}}\right) \tag{8}$$

where $\alpha = k_e/C$ and C is the mean heat capacitance that includes the effect of latent heat. Accordingly, Eq. (8) is also the solution of Eq. (7a) only when $r = 1$.

3.1. Estimation of the location of phase front

To demonstrate the effect of the moving front, the data in Figs. 4 and 5 are re-plotted having x as the abscissa. For various times, t, the temperature distribution in the direction perpendicular to the plane of the applied heat load is presented in Figs. 6 and 7. For the purpose of estimating the arrival of the melting front at any preselected site, a horizontal dash line is drawn across each of the plots at the melting point of the PCM. This line demarcates the solid and the liquid region, and it indicates the arrival of the phase change front at any given location and time when $T_s \cong T_m$. This is evident in Fig. 4 for the location 7.5 mm, where there is a temperature

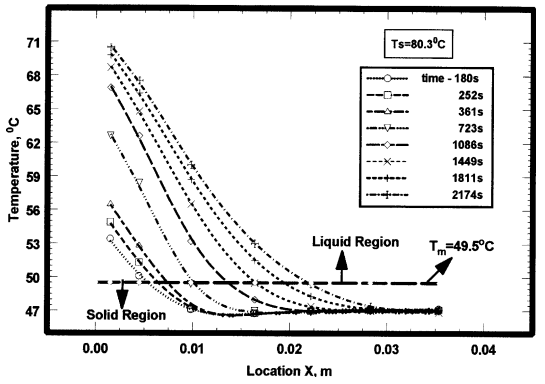

Fig. 6. Variation of temperature with location, PCM-saturated porous medium, surface temperature $T_0 = 80.3$ °C.

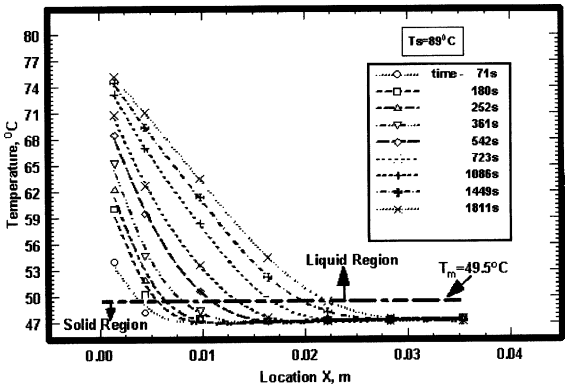

Fig. 7. Variation of temperature with location, PCM-saturated porous medium, surface temperature $T_0 = 89$ °C.

jump due to the arrival of the melting front. The temperature jump is not seen at the location 1.5 and 4.46 mm; they are in immediate neighborhood of the wall since the solid matrix is composed of 3 mm spheres. This is attributed to the limitations in the response of the temperature sensor to changes in temperature over a short period. As expected, the temperature jump is not noticeable in the far-field region since the melting process is much slower, and $T_s \cong T_p$. In reality, the fully solid and the fully liquid region may be separated by melting or mushy region. Below and above the dash line are the solid and the liquid regions, respectively. The solid region contains the solid matrix and the solid phase PCM, and the liquid region consists of the solid matrix and the liquid PCM and may include the mushy zone. It can be seen from Figs. 6 and 7, well above and below the melting point, that the temperature variation with location is approximately linear. In these regions, one can hypothesize that the solid matrix is in thermal equilibrium with the pore materials; hence the one-temperature equation model is adequate to predict the temperature response of the porous medium to thermal perturbation. However, in the neighborhood of the melting temperature, 49.5 °C, the temperature distribution is non-linear. In this region, when $T_s > T_m$, which is the mushy or melting region, the pore material is undergoing the phase change process and the temperature of the solid matrix remains higher than the pore temperature until the phase change process is complete, see Figs. 6 and 7. Because of the temperature difference between the solid matrix and the pore material, the two-temperature equation model is best suited for analyzing the thermal behavior in this region.

The location of the melting front is estimated using data obtained from Figs. 6 and 7. In Figs. 6 and 7, the point of intersection of the dashed horizontal line with each of the plots indicates the location of the melting front at a given time. Fig. 8 presents the measured location of the melting front $X(t)$ with time for $T_0 = 64.2$, 71.6, 80.3, and 89 °C. The symbols in Fig. 8 represent the experimentally predicted phase fronts while the lines represent expected asymptotic behavior of the data related to the time t, in the form $X \sim t^{0.5}$, under LTE condition. The experimental data in Fig. 8 clearly show that those for $T_0 = 89.0$ °C are well below the dot–dot line and the data for $T_0 = 80.3$ °C are well below the dot–dash line, especially at smaller times. This tendency is also detectable from data for other surface temperatures listed in Fig. 8. Indeed, all data approach LTE condition as time increases. Therefore, this figure hints toward the possibility having a LTNE condition and deserves further investigation.

An examination of data from Fig. 8 indicates that the phase front departs from its LTE condition especially during the early stage of the melting process while their trend is consistent with theoretical information at larger

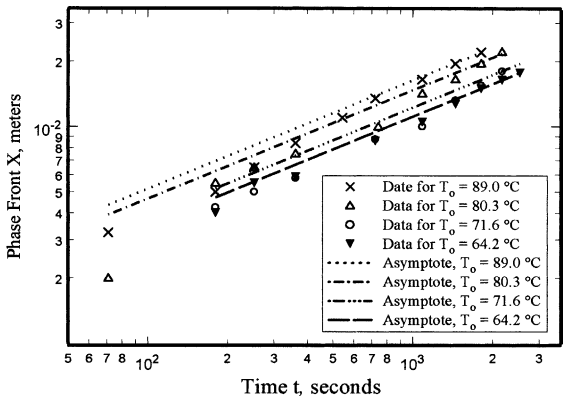

Fig. 8. Measured phase front as a function of time for different T_0 and expected LTE condition.

time. Because, the theoretical studies in Harris et al. [12] show that when t is large, the phase front approaches local thermal equilibrium condition; that is

$$X = 2k_e(T_0 - T_m)\sqrt{t}/(\rho L\sqrt{\pi\alpha}) \tag{9}$$

for all combinations of τ_t and τ_q. Before the formation of the liquid melt, the energy transferred to the porous medium is consumed in the form of sensible heat. Upon formation of the liquid melt layer, heat delivered to the porous medium is partly stored in the liquid and solid region as sensible heat and partly as latent heat at the liquid–solid interface. At larger times, the solid temperature near the phase front reduces and therefore the rate of change of the phase front decreases. This is responsible for the near LTE condition at a large time.

Since the capacitance is a thermophysical property, it is independent of the boundary condition. Harris et al. [12] used the boundary condition $T_p = T_0$ at $x = 0$ to facilitate the theoretical estimation of the mean heat capacitance C. Accordingly, the mean capacitance [12] defined as

$$C \cong \frac{\pi\rho L}{2(T_0 - T_m)} \tag{10}$$

and the definition of the dimensionless moving front X^*, Eq. (6), is obtained using this relation. This relation is valid because there is a near LTE condition at $x = 0$ except for a very small time. Once the value of C is determined, the boundary condition at $x = 0$ need to be modified by assuming $T = T_s$ at $x = 0$. This is necessary because heat transfers primarily into solid matrix and then to phase change materials. However, in the experimental setup discussed earlier, heat does indeed transfer directly from the wall to the phase change materials and this can affect the speed of the moving front at extremely small times.

3.2. Modified theoretical predictions

It is appropriate to compute the variation of the temperature field as the front passes specific locations. When the material domain is initially at temperature T_m, in one-dimensional space, a solution for Eq. (5) is possible. Using a dimensionless temperature $\theta_p = (T_p - T_m)/(T_0 - T_m)$, the solution by the Laplace transform method, assuming $T_s = T_0$ at $x = 0$, leads to the relation

$$\bar{\theta}_p = L_p\{\theta_p\} = \frac{1}{s(rs+1)} e^{-\sqrt{s(s+1)/(rs+1)}\xi} \tag{11}$$

where s is the Laplace transform variable, L_p is the Laplace operator, $\xi = x/\sqrt{\alpha\tau_a}$. In the derivation of Eq. (11) it is necessary to have $\bar{\theta}_p$ at $\xi = 0$. The Laplace transform of Eq. (5b) provided the condition $\bar{\theta}_p(0,s) = 1/[s(rs+1)]$. In practice, it is possible to obtain the inverse Laplace transform of Eq. (11) numerically. Moreover, Eq. (5b) yields the dimensionless temperature of the solid matrix also in the Laplace transform space as

$$\bar{\theta}_s = \bar{\theta}_p + \frac{r}{(rs+1)} e^{-\sqrt{s(s+1)/(rs+1)}\xi} \tag{12}$$

where $\theta_s = (T_s - T_m)/(T_0 - T_m)$. Once the region at and near the wall reaches to LTE condition, most of the heat flux at the wall is consumed as latent heat since the sensible heat portion becomes small. Then, it is acceptable to use the relation $-(k_e \partial T_p/\partial x)|_{x=0} = \rho L \partial X/\partial t$. This relation, in conjunction with Eqs. (6) and (11), yields

$$L_p\{X^*\} = \frac{\sqrt{s(s+1)/(rs+1)}}{s^2(rs+1)} \tag{13}$$

in the Laplace transform space. The inverse Laplace transform Eq. (13) is

$$X^* = \frac{1}{\sqrt{\pi r^3}} \int_{\tau=0}^{\eta} [(\eta-\tau)^{-1/2} + 2(\eta-\tau)^{1/2}] \times \exp\left(-\frac{r+1}{2r}\tau\right)\left[I_0\left(\frac{r-1}{2r}\tau\right) + I_1\left(\frac{r-1}{2r}\tau\right)\right]\tau \, d\tau \tag{14}$$

In this study, for all other values of r, the values of X^* are obtained through numerical integration of Eq. (14). In the subsequent analysis, the following parameters remain unchanged: $\rho = 796$ kg/m^3 and $k_e = 0.55$ W/m K. The effective latent heat of fusion L in Eq. (10) is viewed as an unknown during the following parameter estimation. It needs to be estimated because it should be different from 255 kJ/kg, for pure tetracosane, for the following reasons: At $x = 0$, according to Eq. (10), T_0 is the temperature of the pore materials whereas, in this experimental study, T_0 is the solid matrix temperature. The expected value of L should be less than 255 kJ/kg since the porosity ε is less than 1 and it should be larger than 255ε kJ/kg due to existence of the mushy zone behind the front. The other parameters to be estimated are τ_t and τ_q.

3.3. Parameter estimation

The objective is to identify a best set of τ_t, τ_q, and L that minimizes the standard deviation defined as

$$SD = \sqrt{\frac{1}{N-1}\sum_{n=1}^{N}[(x)_{measured} - (x)_{calculated}]^2} \tag{15}$$

The process begins by providing estimated values for τ_t, τ_q, and L. A proper initial estimate for the effective latent heat is 184 kJ/kg, the mid point between 255ε and 255 kJ/kg. Minkowycz et al. [13] presented a relation $\tau_q \approx C_s R_c \Delta V_s/\Delta A_s$ to estimate the value of this parameter. For a loosely packed bed, the contact resistance R_c depends on the geometry of the solid region and the thermal conductivity of material in the pores. This value of τ_q for a similar porous medium, except, the pores are filled with air, is reported in Nnanna et al. [20]. Assuming the contact region is filled with liquid tetracosane instead of air, the thermal conductivity ratio yields an initial estimate for $\tau_q = 50$ s. The parameter τ_t, as defined in Ref. [13], is a local quantity related to the interstitial heat transfer coefficient; therefore, the conductance in its definition is also a local quantity related to the latent heat of fusion of the tetracosane in the pores. A crude method of estimating τ_t is to use $hr_h/k_e = 2/3$ and get $\tau_t \sim (\rho L)_p r_h/[h(T_s - T_m)]$ with $T_s - T_m \approx 4$–5 °C. Using Eq. (15) and an iterative procedure, these three values are computed as $\tau_t = 60.1$ s, $\tau_q = 47.3$ s, and $L = 208.9$ kJ/kg. Fig. 9 shows the variation of these

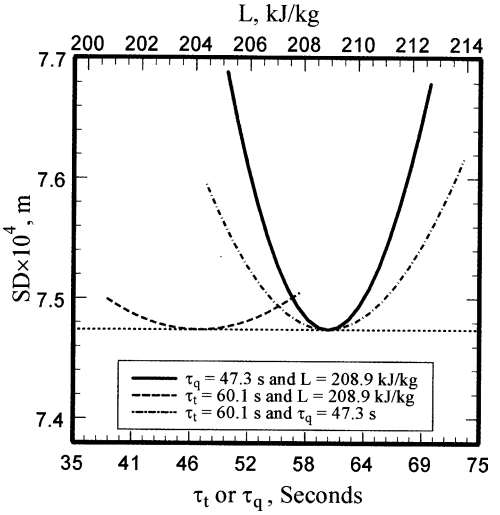

Fig. 9. Variation of standard deviation with τ_t, τ_q and k_e.

parameters and their effect on the standard deviation SD. This figure shows that the influence of τ_q on SD is less than that of τ_t. According to the data plotted in this figure, the minimum value of SD is 0.0007477 for the entire set of data. Using the estimated L, τ_t and τ_q, the values of τ_a computed using $\tau_a = \tau_q + C_s\tau_t/C$ for the surface temperatures of $T_0 = 64.2$, 71.6, 80.3, and 89 °C are 52.7, 55.4, 58.5, and 61.8 s, respectively. These, in addition to $r = \tau_t/\tau_a$, with $\tau_t = 60.1$ s, provided the input for a theoretical prediction of the dimensionless location of a moving phase front X^*, see Eq. (14).

Fig. 10 is prepared to show the variation of X^* as a function of $\eta = t/\tau_a$ for data in Fig. 8 when $T_0 = 89.0$ °C. The dotted line shows the theoretically predicted values using $r = 0.973$ and the dash lines indicate ±10% deviation from the predicted values. The standard deviation for this set of data is 0.00054. The solid line depicts the theoretical values of X^* in the presence of LTE. Indeed, Fig. 10 shows that, at large time, the data converge to a limiting value. The data are within a ±10% error band also plotted in Fig. 10 except for a single data taken at a very small time. This is an expected deviation due to relatively larger experimental uncertainties and the limitations of the theoretical model due to direct energy transport from wall to PCM and lack of LTE at $x = 0$ at very small time. However, for $T_0 = 80.3$ °C in Fig. 11, the phase front data at the smallest time exhibits a lesser deviation from the theoretical prediction. Fig. 11 is prepared similar to Fig. 10 except there are four lines for the four predicted X^* values, one set for each surface temperature. Overall, the data for different surface temperatures are in remarkably good agreement with their corresponding theoretically predicted lines for this complex phase change study.

This information points toward the LTNE condition at small time by examining the Sparrow number, $Sp = \overline{C}_p X^2/(\tau_t k_e)$ where X assumes the role of L in the definition of the Sparrow number [13]. Over the range of

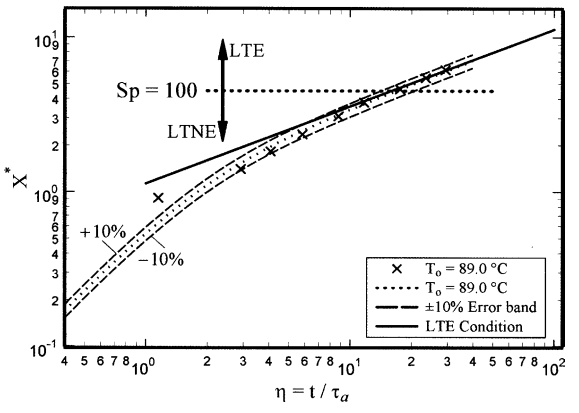

Fig. 10. Comparison of experimental data with theoretical model when $\tau_q = 59.0$ s, and $\tau_t = 64.9$ s.

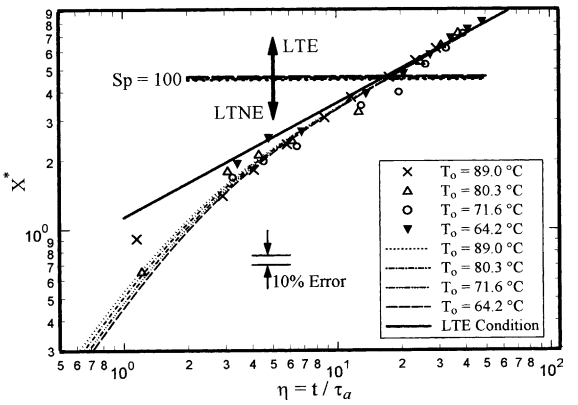

Fig. 11. Variation X^* of as a function of t/τ_a and comparison with theoretical model when $\tau_q = 59.0$ s, and $\tau_t = 64.9$ s.

reported X values, Sp varies between 1.95 and 178 when $T_0 = 89$ °C and varies between 12 and 275 when $T_0 = 64.2$ °C. This attests that Sp can be sufficiently small to induce a LTNE condition. Indeed, the sparrow number is directly related to X^* through the relation

$$Sp = \left(\frac{\overline{C}_p}{C}\right)\left(\frac{\pi}{2}\frac{X^*}{\sqrt{r}}\right)^2 \tag{16}$$

where $\overline{C}_p/C$ is a constant for a given $(T_0 - T_m)$ value. This indicates that the state of LTE will be achieved rapidly since the Sparrow number increases with the square of a dimensionless phase front. The study presented in Minkowycz et al. [13] indicates the arrival of LTE when $Sp > 100$. Indeed, $Sp = 100$ does provide a means to predict the critical X^* values. These critical X^* values for $T_0 = 64.2$, 71.6, 80.3, 89 °C are 4.66, 4.60, 4.55, and 4.51, respectively. Fig. 10 depicts the critical $X^* = 4.51$ while Fig. 11 contains all four critical X^* lines, each corresponding to a given surface temperature; the four lines in Fig. 11 are nearly superimposed. The data in Fig. 11 show that $Sp = 100$ represents a reasonable critical Sparrow number for this application. Because, the data clearly move away from LTE, depicted as a solid line in the figure, as X^* reduces to below the corresponding critical X^* indicating the occurrence of the state of LTNE condition.

Finally, it is appropriate to demonstrate the difference between T_p and T_s under LTNE condition. For two thermocouple locations, $x = 3.25$ and 8.40 mm, the dimensionless temperatures θ_p and θ_s are computed and plotted in Fig. 12. A special commercial Mathematica package [21,22] performed the task of finding the inverse Laplace transforms of Eqs. (11) and (12). The solid lines in the figure correspond to the temperature of the solid matrix and the dash lines represent the temperature of materials in the pores. Fig. 12a is for $x = 3.25$ mm and it shows a larger temperature difference than that for $x = 8.40$ mm plotted in Fig. 12b. Fig. 12a clearly shows

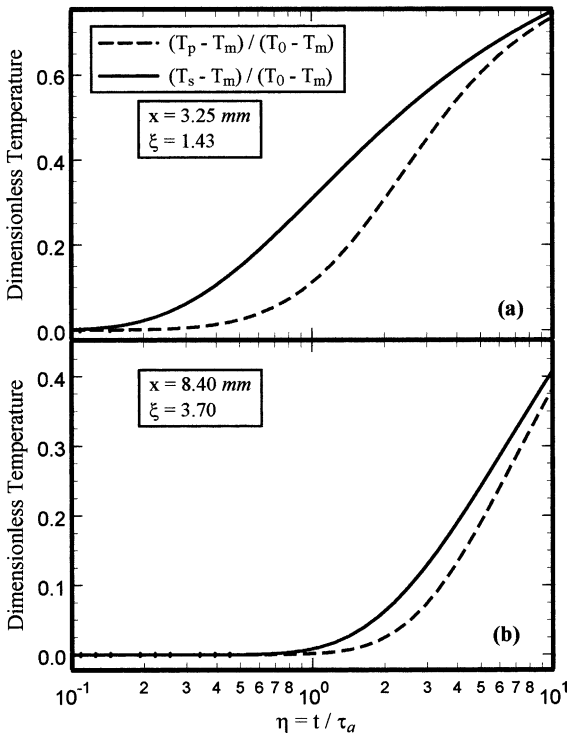

Fig. 12. Predicted mean pore temperature and solid matrix temperature at two locations for data in Fig. 10.

that the phase front arrives at the $x = 3.25$ mm location before it arrives at the $x = 8.40$ mm location in Fig. 12b while the LTE condition arrives faster in Fig. 12b than Fig. 12a.

4. Conclusions

A systematic method of studying the LTNE behavior in PCM-saturated porous media has been experimentally investigated. The measured location phase front served to estimate the coefficients that affect heat transfer during the phase change process; they are: the effective latent heat L, the contribution of the interstitial heat transfer coefficient τ_t, and the effect of the contact/constriction resistance. These measured quantities lead toward compelling experimental evidence of local thermal non-equilibrium phenomena during phase change process in porous media. Experimental evidence in Fig. 8 indicates that there is a departure from the LTE condition during the phase change. The overall results of this study clearly show that for the data at small time, plotted in Fig. 11, and for times smaller than those shown here, there is a departure from local thermal equilibrium. This finite time needed to arrive to LTE is as a result of substructural thermal interaction between the solid matrix and the pore material.

It is observed that as Sp increases to above 100, the near LTE condition will rapidly be enhanced. As Sp moves to below 100, the deviation from LTE condition becomes larger and LTNE is more noticeable. Accordingly, the Sparrow number can provide a guide that would signal the onset of the LTNE condition. For many applications, under LTNE condition, one can get reasonably accurate values of the phase front X from theoretical considerations.

The extent of the phase front X was determined based on experimental data. The validity of the phase front X and the equivalent volumetric heat capacitance C developed in the theoretical model in Harris et al. [12] can serve as a useful tool when analyzing the experimental data. This study also shows that both experimental and analytical predictions are in good accord. Therefore, in the absence of experimental data, the theoretical study, reported in Harris et al., is a viable method of evaluating the melting or freezing process in porous media.

References

[1] J.L. Masur, A.J. Cornie, C.M. Flemings, Infiltration of fibrous preforms by pure metal, Part 1, Theory, Metall. Trans. (20A) (1988) 2535–2547.
[2] L.S. Yao, J. Prusa, in: J.P. Hartnett, T.F. Irvine Jr. (Eds.), Melting and Freezing Advances in Heat Transfer, Academic Press, San Diego, 1989, pp. 1–95.
[3] E.A. Ellinger, C. Beckermann, Melting of a pure substance in an enclosure partially occupied by a horizontal porous layer, ASME HTD Transport Phenom. Mater. Process. 132 (1990) 9–16.
[4] C. Beckermann, E.A. Ellinger, On the effect of porous layers on melting heat transfer in an enclosure, Exp. Heat Transfer 4 (5) (1991) 619–629.
[5] M. Song, R. Viskanta, Lateral freezing of an anisotropic porous medium saturated with an aqueous salt solution, Int. J. Heat Mass Transfer 44 (4) (2001) 733–751.
[6] T. Lucas, J.M. Chourot, Ph Bohuon, D. Flick, Freezing of a porous medium in contact with concentrated aqueous freezant: numerical modeling of coupled heat and mass transport, Int. J. Heat Mass Transfer 44 (11) (2001) 2093–2106.
[7] M. Sahraoui, M. Kaviany, Slip and no-slip temperature boundary conditions at interface of porous, plain media, Int. J. Heat Mass Transfer 35 (4) (1992) 927–943.
[8] M. Sahraoui, M. Kaviany, Slip and no-slip temperature boundary condition at interface of porous, plain media I: conduction, Int. J. Heat Mass Transfer 36 (4) (1993) 1019–1033.
[9] M. Sahraoui, M. Kaviany, Slip and no-slip temperature boundary condition at the interface of porous, plain media: convection, Int. J. Heat Mass Transfer 37 (6) (1994) 1029–1044.
[10] A.J. Ochoa-Tapia, S. Whitaker, Heat transfer at the boundary between a porous medium and a homogeneous fluid, Int. J. Heat Mass Transfer 40 (11) (1997) 2691–2707.

[11] K. Vafai, M. Sozen, Analysis of energy and momentum transport for fluid flow through a porous bed, J. Heat Transfer 112 (3) (1990) 690–699.
[12] K.T. Harris, A. Haji-Sheikh, A.G.A. Nnanna, Phase change phenomena in porous media—a non-local thermal equilibrium model, Int. J. Heat Mass Transfer 44 (2001) 1619–1625.
[13] W.J. Minkowycz, A. Haji-Sheikh, K. Vafai, On departure from local thermal equilibrium in porous media due to a rapidly changing heat source: the Sparrow Number, Int. J. Heat Mass Transfer 42 (18) (1999) 3373–3385.
[14] D.Y. Tzou, Macro-to-Microscale Heat Transfer: The Lagging Behavior, Taylor & Francis, Washington, DC, 1997.
[15] A.A. Tarzimanov, F.R. Gabitov, I.N. Ponikarova, F.D. Yuzmukhametov, Application of pulse heating method for various thermal studies, Inzhenerno-Fizicheskii Zhuenal 63 (4) (1992) 436–441.
[16] S. Gustafsson, E. Karawacki, J.K. Kruger, M. Pietralla, Thermal conductivity of *n*-Tetracosane around the liquid–liquid transition temperature, Colloid Polym. Sci. 263 (7) (1985) 603–606.
[17] S. Himran, A. Suwondo, G. Mansoori, Characterization of alkanes and paraffin waxes for application as phase change energy storage medium, Energy Sources 16 (1) (1994) 117–128.
[18] A.G.A. Nnanna, Phase Change Phenomena in Porous Medium: A Local Thermal Non-Equilibrium Study, Ph.D. Dissertation, The University of Texas at Arlington, Arlington, TX, USA, 2002.
[19] K. Kaviany, Principles of Heat Transfer in Porous Media, Springer-Verlag, New York, 1991.
[20] A.G.A. Nnanna, A. Haji-Sheikh, K.T. Harris, An experimental study of non-Fourier thermal response in porous media, J. Porous Media, in press.
[21] S. Wolfram, The Mathematica Book, fourth ed., Cambridge University press, Cambridge, UK, 1999.
[22] P.P. Valkó, S. Vajda, Inversion of noise-free Laplace transforms: towards a standardized set of test problems, Inverse Problems Eng. 10 (5) (2002) 467–483.